Journal of Solid State Chemistry 183 (2010) 361–366

Contents lists available at ScienceDirect

Journal of Solid State Chemistry

journal homepage: www.elsevier.com/locate/jssc

Synthesis, crystal structure, and photocatalytic activity of the new three-layer aurivillius phases, $Bi_2ASrTi_2TaO_{12}$ (A=Bi, La)

Dong Wang [a,b,*], Kaibin Tang [a,b], Zhenhua Liang [a,b], Huagui Zheng [b]

[a] Nanomaterial and Nanochemistry, Hefei National Laboratory for Physical Sciences at Microscale, University of Science and Technology of China, Hefei, Anhui 230026, PR China
[b] Department of Chemistry, University of Science and Technology of China, Hefei, Anhui 230026, PR China

ARTICLE INFO

Article history:
Received 31 July 2009
Received in revised form
25 October 2009
Accepted 22 November 2009
Available online 3 December 2009

Keywords:
Perovskite
Aurivillius phase
Powder X-ray diffraction
Photocatalysis

ABSTRACT

Two new three-layer Aurivillius phases $Bi_2ASrTi_2TaO_{12}$ (A=Bi, La) have been synthesized. The detailed structure determination of $Bi_2ASrTi_2TaO_{12}$ (A=Bi, La) performed by powder X-ray diffraction (XRD) and selected area electron microscopy (SAED) shows that they all crystallize in the space group $I4mmm$. UV–visible diffuse reflection spectrum of the prepared $Bi_2ASrTi_2TaO_{12}$ (A=Bi, La) indicates that it had absorption in the ultraviolet (UV) region. The photocatalytic activity of the $Bi_2ASrTi_2TaO_{12}$ (A=Bi, La) powders was evaluated by degradation of rhodamine B (RB) molecules in water under UV light irradiation. The results showed that $Bi_2ASrTi_2TaO_{12}$ (A=Bi, La) has high photocatalytic activity at room temperature. Therefore, the preparation and properties studies of $Bi_2ASrTi_2TaO_{12}$ (A=Bi, La) with a three-layer Aurivillius structure suggest potential future applications in photocatalysis.

1. Introduction

The Aurivillius crystal structure was first discovered by Aurivillius about 60 years ago [1]. It has a general formula $Bi_2O_2[A_{n-1}B_nO_{3n+1}]$, where the structure consists of n perovskite layers separated by $[Bi_2O_2]^{2+}$ sheets along the c-axis, giving a characteristic layered structure. The 12-fold perovskite A sites can be occupied by cations such as Bi^{3+}, Ca^{2+}, Sr^{2+}, Ba^{2+}, La^{3+}, Pb^{2+}, K^+ [1–4], and the 6-fold B site is typically occupied by Ti^{4+}, Nb^{5+}, Ta^{5+}, W^{6+} or Mn^{3+} [1,2,5–7], etc.

Most of Aurivillius structure oxides are known as ferroelectric materials exhibiting high Curie temperatures and large spontaneous polarizations [8–10]. And Aurivillius phases have also found other interesting properties or applications such as photoluminescence device [11], ion exchange and intercalation behavior [12–14], etc. Recently, it was found that Aurivillius structure oxides are efficient photocatalysts for water splitting or organic compounds degradation because of their d^0 electron configuration of transition metal (Ti^{4+}, Nb^{5+}, Ta^{5+}, etc.). For example, Kim et al. discovered that $PbBi_2Nb_2O_9$ is an efficient photocatalyst for water splitting into O_2 or H_2, isopropyl alcohol degradation to CO_2, and production of photo photocurrent, all under visible light [15]. A typical series of Aurivillius phases $Bi_2Mo_nO_{3n+3}$ (n=1–3) were also reported to have a good activity for water decomposition and organic compounds degradation under visible-light irradiation [16–18]. All of these revealed that Aurivillius structure oxides are potential photocatalytic materials in the future.

Up to the present, besides $Bi_4Ti_3O_{12}$, some Aurivillius phases with triple-layered perovskite-like slabs have been reported. Such as $Bi_{4-x}Ln_xTi_3O_{12}$ (Ln=La, Pr, Nd, and Sm-Lu) [19–22], $Bi_2Sr_{2-x}A_xNb_2TiO_{12}$ (A=Ca, Ba; x=0, 0.5, 1) [22–24], $Bi_{2-x}Sr_{2+x}B_{2+x}M_{1-x}O_{12}$ (B=Nb, Ta; M=Ru, Ir, Mn; x=0, 0.5) [25,26], $Bi_2ANaB_3O_{12}$ (B=Nb, Ta; A=Sr, Ca) [27]. However, in these papers, for three-layer Aurivillius phases, their photocatalytic activities were scarcely investigated and discussed.

In the present work, two new three-layer Aurivillius phases, $Bi_2ASrTi_2TaO_{12}$ (A=Bi, La) were successfully prepared, as very active photocatalysts. Detailed powder X-ray diffraction and selected area electron microscopy (SAED) study of $Bi_2ASrTi_2TaO_{12}$ shows they all crystallizes in the space group $I4/mmm$. Photocatalytic activity is characterized by diffuse reflectance UV–vis spectroscopy and degradation of rhodamine-B (RB) molecules in water under ultraviolet (UV) light irradiation.

2. Experimental section

2.1. Preparation of samples

Polycrystalline samples of $Bi_2ASrTi_2TaO_{12}$ (A=Bi, La) were prepared by a conventional solid state reaction method. All reagents were analytically pure and used without further

* Corresponding author at: Department of Chemistry, University of Science and Technology of China, Hefei, Anhui 230026, PR China.
E-mail addresses: dwang@mail.ustc.edu.cn (D. Wang), kbtang@ustc.edu.cn (K. Tang).

0022-4596/$ - see front matter © 2009 Elsevier Inc. All rights reserved.
doi:10.1016/j.jssc.2009.11.018

purification. Stoichiometric amounts of Bi_2O_3, La_2O_3, $SrCO_3$, TiO_2 and Ta_2O_5 were ground together, pressed into pellets, and preheated at 800 °C for 24 h in order to prevent melting of Bi_2O_3. Then the mixed powders were calcined in air at 1100 °C for 48 h with intermediate grindings (heating rate 10 °C/min).

2.2. Samples characterizations

Phase analysis of the products was examined by X-ray powder diffraction (XRD) using a Philips X'pert Pro Super diffractometer equipped with graphite monochromatized Cu$K\alpha$ radiation (λ=1.54178 Å) at room temperature (40 kV, 30 mA). The XRD data for indexing and cell-parameter calculation were collected in a continuous scan mode with a step size of 0.017 °C in the angular range $5<2\theta<110^\circ$. The XRD patterns were analyzed by the Rietveld method using the FULLPROF program [28].

The structures of the prepared samples were further examined with selected area electron microscopy (SAED). Powered samples of the $Bi_2ASrTi_2TaO_{12}$ (A=Bi, La) compounds were ground and ultrasonicated in absolute ethanol, and then a drop of the diluted colloidal suspension of the samples was placed onto a Cu grid. After being air-dried, the samples were subjected to ED observations on a JEOL-2010 transmission electron microscope at an acceleration voltage of 200 kV. UV–vis diffuse reflectance spectrums (DRS) of the samples were measured using a Hitachi U-3010 UV–vis spectrophotometer.

2.3. Photocatalytic test

Photocatalytic activities of the $Bi_2ASrTi_2TaO_{12}$ powder were evaluated by the degradation of rhodamine-B (RB) solution under UV light. In a typical process, 100 mg of $Bi_2ASrTi_2TaO_{12}$ powder was added to 100 mL of a 1.0×10^{-5} M Rhodamine B (RB) solution and then magnetically stirred in the dark for 15 min, which allowed it to reach adsorption equilibrium and uniform dispersity. The solution was then exposed to UV irradiation from a 250 W high-pressure Hg lamp at room temperature. The samples were collected by centrifugation every 20 min to measure the RB degradation by UV–vis spectra (Shimadzu UV2550).

3. Results and discussion

3.1. Structure characterization of $Bi_2ASrTi_2TaO_{12}$

The X-ray diffraction profiles of all samples reveal that no impurities exist in the compounds. All peaks of the XRD patterns (in the angular range $10^\circ<2\theta<60^\circ$) could be indexed on a tetragonal cell, and the systematic absences showing body-centering leading to an I-extinction symbol.

In order to confirm the result obtained from the X-ray diffraction experiment. The 3D reconstruction of the reciprocal lattice of $Bi_2ASrTi_2TaO_{12}$ was performed form SAED patterns. They are shown in Fig. 1 ([001] and [100] zone axis patterns of $Bi_2LaSrTi_2TaO_{12}$) and Fig. 2 ([001] and [100] zone axis patterns of $Bi_3SrTi_2TaO_{12}$). All of the observed reflections can be indexed with a tetragonal lattice ($a=b\approx3.9$ Å and $c\approx33$ Å for both compounds). And from all patterns only reflections satisfying an $h+k+l=2n$ conditions are present. These results are in good agreement with those obtained from the X-ray diffraction study. The existence conditions together with the X-ray diffraction patterns suggest that two compounds all crystallize in the tetragonal space group $I4/mmm$ which is similar to $Bi_2Sr_2Nb_2TiO_{12}$ [23].

However, in an early study of three-layer Aurivillius phases, $Bi_2SrANb_2TiO_{12}$ (A=Ca, Ba), Zhou et al. have indicated that compared with $I4/mmm$, the space group $B2cb$ is more suitable for their compounds [24]. And we attempted using the lower symmetry space group $B2cb$, but could not obtain a stable refinement for our compounds. It seems that the orthorhombic distortion in our compounds is too weak to be characterized by X-ray diffraction. However, the $I4/mmm$ model proved more reasonable for our compounds. So we choose for X-ray diffraction, the space group $I4/mmm$ for the determination of the average structure. The structure was refined by the Rietveld technique using all data of XRD above 10° (2θ) because of the high asymmetry of background at low angles.

In the refinement, some problems were found. Firstly, for $Bi_3SrTi_2TaO_{12}$, initial attempts to refine the data with the alkaline earth adopting a more isotropic position different from Bi^{3+} resulted in an unreasonable atomic position of Sr^{2+} (Bi site). Secondly, the isotropic atomic displacement parameter (Biso) of O (1) is unreasonably large and O (4) is negative for both compounds. So to obtain a stable refinement, several constraints were introduced: (a) For $Bi_3SrTi_2TaO_{12}$, the atomic position of Bi^{3+}/Sr^{2+} in the Bi site were constrained to be equivalent, although we knew the clear preference of Sr^{2+} for a more symmetrical environment than Bi^{3+} because of the lack of the lone pair of electrons. (b) According to the structure model proposed by Neil C. Hyatt et al. [21] for $Bi_2Ln_2Ti_3O_{12}$ (Ln=La, Pr, Nd and Sm), the O (1) oxygen atom is allowed to displace from the ideal 4e position, (1/2, 0, 1/2), to a new 8j position, $(1/2-x, 0, 1/2)$, corresponding to a rotation of Ti (1)/Ta (1) octahedra about the $\langle001\rangle$ axis. (c) For both compounds, the isotropic atomic displacement parameters (Biso) of oxygen atoms constrained to be equivalent. Then the refinements converged quickly, and the isotropic atomic displacement parameters (Biso) of O decrease to a reasonable values. The observed, calculated and difference of the X-ray diffraction pattern for $Bi_2ASrTi_2TaO_{12}$ are given in Figs. 3 and 4, and there is good agreement between the observed and the calculated patterns.

The final atomic parameters for Rietveld powder X-ray refinements of both compounds are listed in Tables 1 and 2 (Table 1: A=La, Table 2: A=Bi). From the refinements, some major structure features were observed. Firstly, in the atomic parameters of $Bi_2LaSrTi_2TaO_{12}$, because of considering the lack of the lone pair of electrons in La^{3+} and Sr^{2+}, the relaxation of the La (1)/Sr (1) when located on the Bi site was observed. Secondly, the site mixing between the perovskite A site and the Bi site was established, as well as mixing among the perovskite B site containing Ti and Ta. This site mixing is common in the Aurivillius phases [19–26]. As pointed out by Armstrong and Newnham [29] the $[Bi_2O_2]$ block constrains the size of the perovskite block. Site mixing, therefore, occurs to equilibrate the lattice dimension between the $[Bi_2O_2]$ block and the perovskite block in the ab plane. These authors suggested an "ideal" a-parameter for a $[Bi_2O_2]$ block to be 3.80 Å, and derived an empirical formula for the a-parameter of an idealized perovskite block $[A_2B_3O_{10}]$,

$$a=1.33r_B+0.60r_A+2.36$$

where r_B represents the six-coordinate cation radius and r_A an eight-coordinate cation radius, taken from Shannon [30]. In this case ionic radii (Å) are Bi^{3+}, 1.17; La^{3+}, 1.16; Sr^{2+}, 1.26; Ti^{4+}, 0.61; Ta^{4+}, 0.64; and mean $[Ti_2Ta]$ 0.62. From above equation, the idealized a-parameter for an ideal $[ASrTi_2TaO_{10}]$ block is calculated to be 3.92 Å (a for A=La and A=Bi is almost equal because of the approximate r_{Bi} and r_{La}), a severe mismatch of the ideal 3.80 Å for $[Bi_2O_2]$ block. Thus site mixing occurs to reduce the strain in the intergrowth. From the above arguments we can

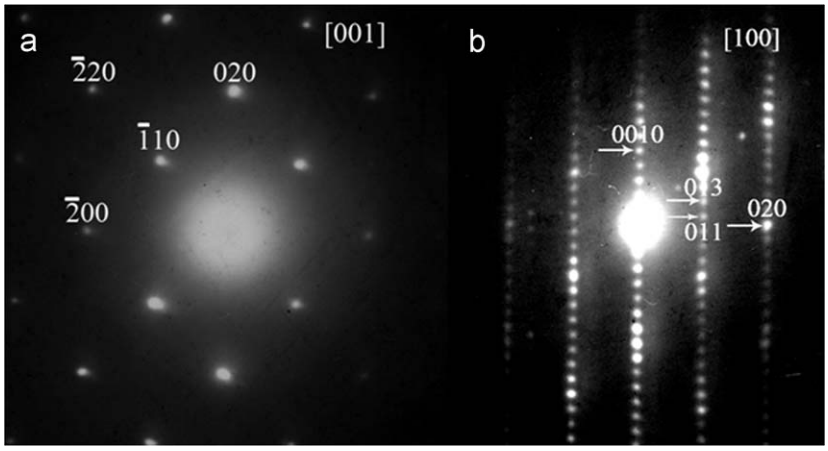

Fig. 1. SAED patterns of $Bi_2LaSrTi_2TaO_{12}$ along (a) [001] and (b) [100].

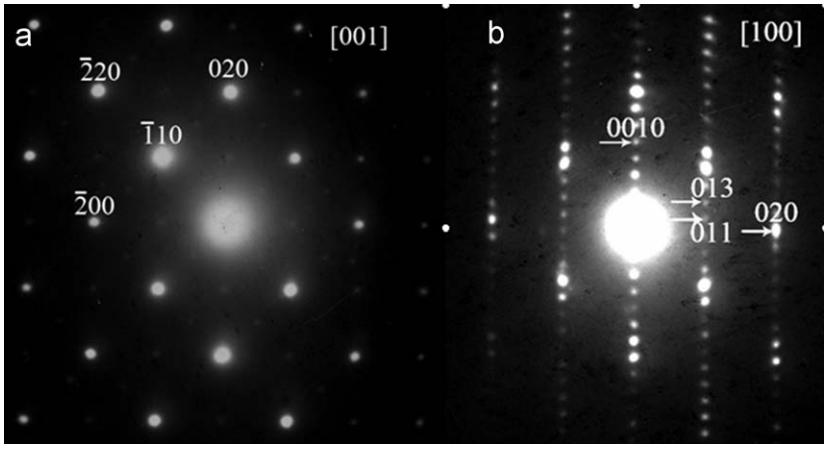

Fig. 2. SAED patterns of $Bi_3SrTi_2TaO_{12}$ along (a) [001] and (b) [100].

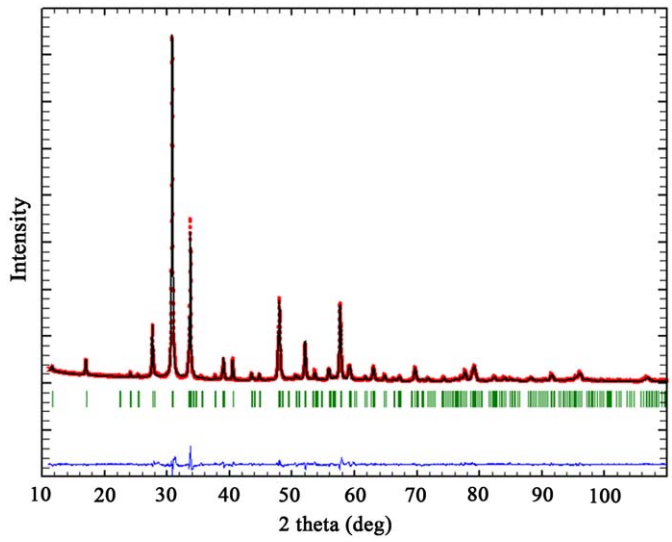

Fig. 3. Observed (dotted line), calculated (solid line) and difference (bottom) powder X-ray diffraction patterns of $Bi_2LaSrTi_2TaO_{12}$ after structural refinements in the space group *I*4/*mmm*. The vertical bars are the Bragg positions of the reflections in the space group *I*4/*mmm*.

also understand the reason of La^{3+} preferring to remain on the *A* site in the $Bi_2LaSrTi_2TaO_{12}$ phase (Table 1). That is because the radius of Bi^{3+} and La^{3+} are almost equal, and substitution of La^{3+} on the Bi site will not reduce the interlayer strain.

Form Tables 1 and 2 another interesting feature could be found: On substituting Bi^{3+} for La^{3+} the most significant change is that the Sr^{2+} site mixing on the Bi site decreases, in other words, the Sr^{2+} in the Bi site is preferentially substituted, rather than the Bi^{3+} going into the *A* site. For $Bi_2LaSrTi_2TaO_{12}$ there is about 18% Bi/*A* site mixing (Sr^{2+}:12%, La^{3+}:6%) which is similar to previous works. However, there is only about 6% Bi/*A* site mixing in the compounds $Bi_3SrTi_2TaO_{12}$. A similar result was also reported in the work of Hervoches and Lightfoot [22]. And this showed that, despite site mixing, the *A* site with more regular environments is more suitable for Sr^{2+}.

Site mixing was also observed on the perovskite *B* sites. From Tables 1 and 2 it was found that a slight preference of Ti for the central site in the block occurs. According to the second-order Jahn-Teller effect, the central site is often more associate with $5d^0$ rather than $3d^0$ element in perovskite *B* sites [31]. However, considering the different groups of Ti^{4+} and Ta^{5+}, ionic charge effects may also play an important role. An increase in the Ta^{5+} content on the Ti site was observed for the $Bi_3SrTi_2TaO_{12}$ phase. The reason is unknown. It may be due to the lone pair of electrons of Bi^{3+}.

A presentation of the $Bi_2ASrTiTaO_{12}$ structure is shown in Fig. 5. And selected bond lengths for $Bi_2ASrTiTaO_{12}$ are presented in Table 3. From the Table 3, a strongly distorted coordination environment for Ti(2)/Ta(2) is revealed, involving a displacement from the center of its octahedron toward the transition-metal layers to give one long Ti(2)/Ta(2)–O(3), one short Ti(2)/Ta(2)–O(4), and four normal length Ti(2)/Ta(2)–O(5) bonds. In

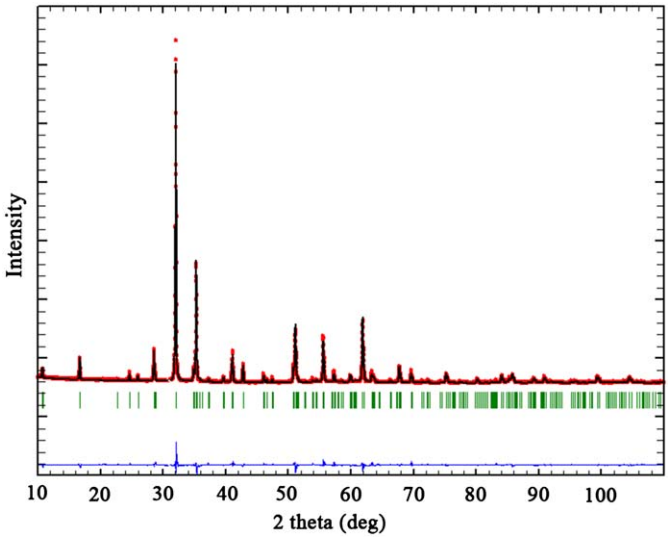

Fig. 4. Observed (dotted line), calculated (solid line) and difference (bottom) powder X-ray diffraction patterns of $Bi_3SrTi_2TaO_{12}$ after structural refinements in the space group *I*4/*mmm*. The vertical bars are the Bragg positions of the reflections in the space group *I*4/*mmm*.

Table 1
The final refined atomic parameters for Rietveld powder X-ray refinements of $Bi_2LaSrTi_2TaO_{12}$ in the space group *I*4/*mmm* (*z*=2) with *a*=3.8623(17) Å, *c*=33.0496(41) Å.

Atom	Site	*g*	*x*	*y*	*z*	B (A2)
Bi(1)	4*e*	0.815(7)	1/2	1/2	0.2133(7)	1.097(37)
Sr(1)	4*e*	0.124(5)	1/2	1/2	0.1936(6)	1.097(37)
La(1)	4*e*	0.059(8)	1/2	1/2	0.1936(6)	1.097(37)
Bi(2)	4*e*	0.184(3)	1/2	1/2	0.0644(6)	2.554(86)
Sr(2)	4*e*	0.375(5)	1/2	1/2	0.0644(6)	2.554(86)
La(2)	4*e*	0.440(2)	1/2	1/2	0.0644(6)	2.554(86)
Ti(1)	2*a*	0.827(8)	0	0	0	0.067(80)
Ta(1)	2*a*	0.172(2)	0	0	0	0.067(80)
Ti(2)	4*e*	0.586(1)	0	0	0.1270(4)	0.399(20)
Ta(2)	4*e*	0.413(9)	0	0	0.1270(4)	0.399(20)
O(1)	8*j*	1/2	0.4065(4)	0	1/2	1.613(33)
O(2)	4*d*	1	1/2	0	1/4	1.613(33)
O(3)	4*e*	1	1/2	1/2	0.4447(7)	1.613(33)
O(4)	4*e*	1	1/2	1/2	0.3244(5)	1.613(33)
O(5)	8*g*	1	1/2	0	0.1166(9)	1.613(33)

*R*p=12.8, *R*wp=12.3, *R*exp=4.77, R_B=4.26, R_F=4.68.

contrast to Ti(2)/Ta(2)O_6 octahedra, a similar bond length of Ti(1)/Ta(1)–O(1) and Ti(1)/Ta(1)–O(3) gives slightly distorted central Ti(1)/Ta(1)–O_6 octahedra. Similar bond characters have been observed in a number of d^0 systems containing niobium, tantalum and titanium. And this has been attributed to a second-order Jahn–Teller effect. [31]. Concerning the bismuth oxide layer, 8-fold Bi(1) have four short Bi(1)–O(2) and four long Bi(1)–O(4) bonds. Due to considering the lone pair of electron of Bi^{3+} in the $Bi_2LaSrTi_2TaO_{12}$, La(1)/Sr(1) in the bismuth oxide layer adopt a more isotropic position. They are closer to O(4) and have four longer La(1)/Sr(1)–O(2) and four shorter La(1)/Sr(1)–O(4) bonds than Bi(1) resulting in a similar bond length of La(1)/Sr(1)–O(2) and La(1)/Sr(1)–O(4). However, because of ignoring the difference of Bi^{3+} and Sr^{2+} in the compound $Bi_3SrTi_2TaO_{12}$, Bi(1) and Sr(1) have an identical atomic position. All the bond lengths are in good agreement with the values in the literature.

Table 4 presents the calculated bond valence sum (BVS) for the four cation sites in the two compounds. Considering the site mixing of Bi and *A*, the BVS for the Bi site and *A* site are reasonable. But the BVS for the Ti/Ta sites are somewhat over-

Table 2
The final refined atomic parameters for Rietveld powder X-ray refinements of $Bi_3SrTi_2TaO_{12}$ in the space group *I*4/*mmm* (*z*=2) with *a*=3.8614(81) Å, *c*=33.1330(57) Å.

Atom	Site	*g*	*x*	*y*	*z*	B (A2)
Bi(1)	4*e*	0.940(5)	1/2	1/2	0.2124(2)	1.503(02)
Sr(1)	4*e*	0.059(5)	1/2	1/2	0.2124(2)	1.503(02)
Bi(2)	4*e*	0.559(5)	1/2	1/2	0.0668(8)	3.886(78)
Sr(2)	4*e*	0.440(5)	1/2	1/2	0.0668(8)	3.886(78)
Ti(1)	2*a*	0.731(8)	0	0	0	0.125(87)
Ta(1)	2*a*	0.268(2)	0	0	0	0.125(87)
Ti(2)	4*e*	0.634(1)	0	0	0.1282(2)	0.987(21)
Ta(2)	4*e*	0.365(9)	0	0	0.1282(2)	0.987(21)
O(1)	8*j*	1/2	0.4291(9)	0	1/2	2.042(71)
O(2)	4*d*	1	1/2	0	1/4	2.042(71)
O(3)	4*e*	1	1/2	1/2	0.4412(1)	2.042(71)
O(4)	4*e*	1	1/2	1/2	0.3208(3)	2.042(71)
O(5)	8*g*	1	1/2	0	0.1194(2)	2.042(71)

*R*p=11.8, *R*wp=10.6, *R*exp=4.47, R_B=5.92, R_F=5.49.

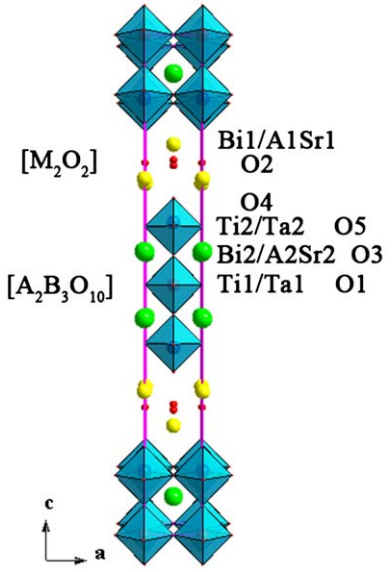

Fig. 5. Schematic structure representation of $Bi_2ASrTi_2TaO_{12}$ (*A*=Bi, La).

bonded. The large BVS in the *B*O6 octahedron has been observed in several three-layer Aurivillius phases $Bi_{1.8}Sr_{2.2}Nb_{2.2}Ti_{1.8}O_{12}$ [22], $Bi_4Ti_3O_{12}$ [32] and $Bi_{2.5}Na_{1.5}Nb_3O_{12}$ [33]. Haluska et al. [21] suggested that it is because of the large O1 and O4 oxygen thermal parameter. In our compounds, the unreasonable and constrained equivalent of O(1) and O(4) oxygen thermal parameter in the refinement is the most possible reason.

3.2. Photoabsorption properties and photocatalytic activity of $Bi_2ASrTi_2TaO_{12}$

It is well-known that light absorption by the material and the migration of the light-induced electrons and holes are the most key factors controlling a photocatalytic reaction, which is relevant to the electronic structure characteristics of the material [34,35]. The UV–vis diffuse reflectance spectra of $Bi_2ASrTi_2TaO_{12}$ are shown in Fig. 6. $Bi_2ASrTi_2TaO_{12}$ presented the photoabsorption properties form the UV-light region to visible light shorter than 450 nm. For a crystalline semiconductor, it was shown that the optical absorption near the band edge follows the equation [36]:

$$\alpha = A(h\nu - Eg)^{n/2}/h\nu$$

Table 3
Selected bond lengths (Å) for $Bi_2ASrTi_2TaO_{12}$.

$Bi_2LaSrTi_2TaO_{12}$		$Bi_3SrTi_2TaO_{12}$	
Bi(1)–O(2)	2.2792(1) × 4	Bi(1)/Sr(1)–O(2)	2.2974(5) × 4
Sr(1)/La(1)–O(2)	2.682(11) × 4	Bi(1)/Sr(1)–O(4)	2.944(4) × 4
Bi(1)–O(4)	3.003(6) × 4	Bi(2)/Sr(2)–O(1)	3.126(14) × 2
Sr(1)/La(1)–O(4)	2.796(5) × 4		2.767(12) × 2
Bi(2)/Sr(2)/La(2)–O(1)	3.128(14) × 2	Bi(2)/Sr(2)–O(3)	2.7436(10) × 4
	2.648(12) × 2	Bi(2)/Sr(2)–O(5)	2.599(5) × 4
Bi(2)/Sr(2)/La(2)–O(3)	2.7482(11) × 4	Ti(1)/Ta(1)–O(1)	1.950(3) × 4
Bi(2)/Sr(2)/La(2)–O(5)	2.590(7) × 4	Ti(1)/Ta(1)–O(3)	1.948(10) × 2
Ti(1)/Ta(1)–O(1)	1.964(4) × 4	Ti(2)/Ta(2)–O(3)	2.300(10) × 1
Ti(1)/Ta(1)–O(3)	1.824(10) × 2	Ti(2)/Ta(2)–O(4)	1.689(10) × 1
Ti(2)/Ta(2)–O(3)	2.374(10) × 1	Ti(2)/Ta(2)–O(5)	1.9527(10) × 4
Ti(2)/Ta(2)–O(4)	1.605(13) × 1		
Ti(2)/Ta(2)–O(5)	1.9612(18) × 4		
Rotation of Ti/Ta(1) octahedral (deg)	5(9)		4(4)

Table 4
Bond valence sum for the two samples.

Site	$Bi_3SrTi_2TaO_{12}$	$Bi_2LaSrTi_2TaO_{12}$
Bi site	2.6	2.7
A site	2.7	2.4
Ti site	4.6	4.4
Ta site	5.1	5.0

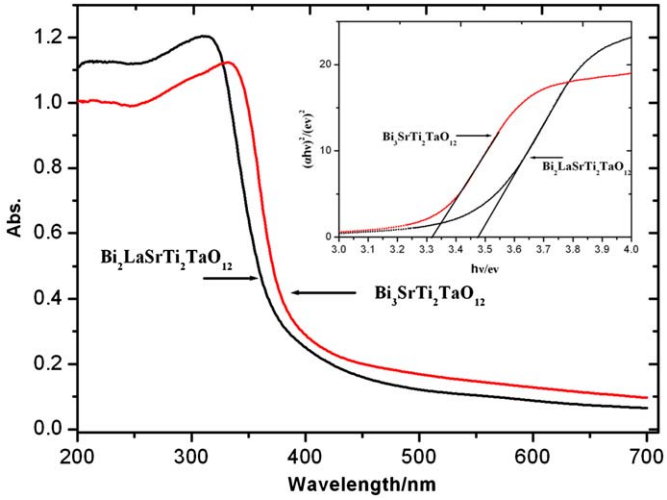

Fig. 6. UV–visible diffuse reflectance spectra of $Bi_2ASrTi_2TaO_{12}$.

where α, ν, Eg, A, and n are the absorption coefficient, incident light frequency, band gap, constant, and an integer, respectively. The integer n depends on the characteristics of the optical transition (n=1, 2, 4 and 6). The value of n as determined for $Bi_2ASrTi_2TaO_{12}$ is 1, indicating that a direct optical transition can occur with no significant change in the wave vector for $Bi_2ASrTi_2TaO_{12}$. The $(\alpha h\nu)^2$ versus $h\nu$ curve of $Bi_2ASrTi_2TaO_{12}$ is illustrated in the inset of Fig. 6. The band gaps of $Bi_2LaSrTi_2TaO_{12}$ and $Bi_3SrTi_2TaO_{12}$ were estimated to be about 3.48 and 3.32 eV, respectively. It is noteworthy that with increasing Bi content the band gap of $Bi_3SrTi_2TaO_{12}$ is smaller than $Bi_2LaTi_2TaO_{12}$. A similar result was also reported in the work of Kim et al. [37]. The empty Ti3*d*, Ta4*d* orbital and the occupied O2*p* orbital are contributing to the formation of conduction and valence bands, respectively, however, the latter is hybridized with Bi6*s*. This hybridization would push up the position of the valence band. With increasing

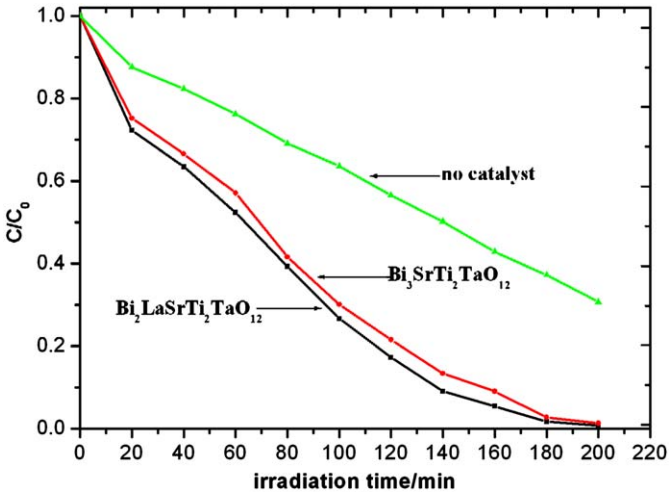

Fig. 7. Photocatalytic degradation of RB over $Bi_2ASrTi_2TaO_{12}$ particles under UV–visible irradiation lights.

Bi content this hybridization also increases, on macroscopically, the band gap decreases.

The photocatalytic activity was evaluated by measuring decomposition rate of rhodamine B (RB) solution at room temperature. Fig. 7 shows the photodegradation curves of RB solution (initial concentration: 1×10^{-5} M, 100 mL) using as-prepared compounds and photocatalyst free under UV–vis light illumination (250 W high-pressure Hg lamp). As is shown, both compounds show a relatively high activity in the reaction. After about 200 min, the RB solutions containing $Bi_2ASrTi_2TaO_{12}$ were almost faded. The decomposition rate of rhodamine B (RB) solution containing $Bi_2ASrTi_2TaO_{12}$ was almost twice faster than that without photocatalyst. Thus, such materials with interesting properties represent good candidates for further applications in the fields of photocatalytic science and technology.

4. Conclusion

In summary, three-layer Aurivillius phases, $Bi_2ASrTi_2TaO_{12}$ (A=Bi, La) have been synthesized. All the compounds crystallize in the space group $I4mmm$. Photocatalytic activity was evaluated by measuring decomposition rate of rhodamine B (RB) solution. And both compounds show a relativity high photocatalytic activity. It is expected that this kind of three-layer Aurivillius structure

$Bi_2ASrTi_2TaO_{12}$ could be exploited for applications in photocatalytic cleaners, optoelectronic devices, water purification, environmental cleaning, and solar energy conversion. This work could be of great importance in extending the potential applications of $Bi_2ASrTi_2TaO_{12}$, a potential advanced functional material.

Acknowledgments

Financial support by the National Natural Science Foundation of China (No. 20621061), the 973 Projects of China and the Program for New Century Excellent Talents in university (NCET) are gratefully acknowledged.

Appendix A. Supplementary material

Supplementary data associated with this article can be found in the online version at doi:10.1016/j.jssc.2009.11.018.

References

[1] B. Aurivillius, Ark. fur Kemi 58 (1949) 499.
[2] S. Blake, M.J. Falconer, M. McCreedy, P. Lightfoot, J. Mater. Chem. 7 (1997) 1609.
[3] T. Rentschler, Mater. Res. Bull. 32 (1997) 351.
[4] N. Yasuda, M. Miyayama, T. Kudo, Solid State Ionics 133 (2000) 273.
[5] R. Macquart, B.J. Kennedy, Y. Shimakawa, J. Solid State Chem. 160 (2001) 174.
[6] R.L. Withers, J.G. Thompson, A.D. Rae, J. Solid State Chem. 94 (1991) 404.
[7] W.J. Yu, Y.I. Kim, D.H. Ha, J.H. Lee, Y.K. Park, S. Seong, H.H. Hur, Solid State Commun 111 (1999) 705.
[8] E.C. Subbarao, J. Chem. Phys. 34 (1961) 695.
[9] R.E. Newnham, R.W. Wolfe, J.F. Dorrian, Mater. Res. Bull. 6 (1971) 1029.
[10] K.R. Kendall, C. Navas, J.K. Thomas, H.C. zur, Loye, Chem. Mater. 8 (1996) 642.
[11] S. Ida, C. Ogata, U. Unal, K. Izawa, T. Inoue, O. Altuntasoglu, Y. Matsumoto, J. Am. Chem. Soc. 129 (2007) 8956.
[12] R.E. Schaak, T.E. Mallouk, Chem. Commun. (2002) 706.
[13] M. Kudo, H. Ohkawa, W. Sugimoto, N. Kumada, Z. Liu, O. Terasaki, Y. Sugahara, Inorg. Chem. 42 (2003) 4479.
[14] S. Taharaa, A. Shimadaa, N. Kumadab, Y. Sugahara, J. Solid State Chem. 180 (2007) 2517.
[15] H.G. Kim, D.W. Hwang, J.S. Lee, J. Am. Chem. Soc. 126 (2004) 8912.
[16] J.C. Jung, H. Lee, H. Kim, Y.M. Chung, T.J. Kim, S.J. Lee, S.H. Oh, Y.S. Kim, I.K. Song, J. Mol. Catal. A Chem. 271 (2007) 261.
[17] Y. Shimodaira, H. Kato, H. Kobayashi, A. Kudo, J. Phys. Chem. B 110 (2006) 17790.
[18] A.M. la Cruz, S.O. Alfaro, E.L. Cuellar, U.O. Mendez, Catal. Today 129 (2007) 194.
[19] R.W. Wolfe, R.E. Newnham, J. Electrochem. Soc. 116 (1969) 832.
[20] M.W. Chu, M.T. Caldes, L. Brohan, M. Ganne, A.M. Marie, O. Joubert, Y. Piffard, Chem. Mater. 16 (2004) 31.
[21] N.C. Hyatt, J.A. Hriljac, T.P. Comyn, Mater. Res. Bull. 38 (2003) 837.
[22] C.H. Hervoches, P. Lightfoot, J. Solid State Chem. 153 (2000) 66.
[23] M.S. Haluska, S.T. Misture, J. Solid State Chem. 177 (2004) 1965.
[24] Q.D. Zhou, B.J. Kennedy, M.M. Elcombe, J. Solid State Chem. 179 (2006) 3744.
[25] W.J. Yu, Y.I. Kim, D.H. Ha, J.H. Lee, Y.K. Park, S. Seong, N.H. Hur, Solid State Commun. 111 (1999) 705.
[26] N. Sharma, C.D. Ling, G.E. Wrighter, P.Y. Chen, B.J. Kennedy, P.L. Lee, J. Solid State Chem. 180 (2007) 370.
[27] W. Sugimoto, M. Shirata, Y. Sugahara, K. Kuroda, J. Am. Chem. Soc. 121 (1999) 11601.
[28] J. Rodriguez-Carvajal, FULLPROF Program: Rietveld Pattern Matching Analysis of Powder Patterns, ILL Grenoble, 1990.
[29] R.A. Armstrong, R.E. Newnham, Mater. Res. Bull. 7 (1972) 1025.
[30] R.D. Shannon, Acta Crystallogr. Sect. A 32 (1976) 751.
[31] N.S.P. Bhuvanesh, J. Gopalakrishnan, J. Mater. Chem. 7 (1997) 2297.
[32] C.H. Hervoches, P. Lightfoot, Chem. Mater. 11 (1999) 3359.
[33] S. Borg, G. Svensson, J.O. Bovin, J. Solid State Chem. 167 (2002) 210.
[34] J.W. Tang, Z.G. Zou, J.H. Ye, Angew. Chem. Int. Ed. 43 (2004) 4463.
[35] J.W. Tang, Z.G. Zou, J.H. Ye, Chem. Mater. 16 (2004) 1644.
[36] J.I. Pankove, Optical Processes in Semiconductors, Prentice-Hall, Englewood Cliffs, NJ, 1971.
[37] H.G. Kim, O.S. Becker, J.S. Jang, S.M. Ji, P.H. Borse, J.S. Lee, J. Solid State Chem. 179 (2006) 1241.